Macromolecules

pubs.acs.org/Macromolecules Article

Conformational Scaling Relations of Two-Dimensional Macromolecular Graphene Oxide in Solution

Peng Li, Shijun Wang, Fanxu Meng, Ya Wang, Fan Guo, Sangeetha Rajendran, Chao Gao, Zhiping Xu,* and Zhen Xu*

Cite This: *Macromolecules* 2020, 53, 10421−10430 Read Online

ACCESS | Metrics & More | Article Recommendations | Supporting Information

ABSTRACT: One of the most celebrated achievements in polymer physics is the finding of simple scaling laws that correlate molecular behaviors with molecular size. Scaling relations of 2D macromolecules between the conformation and size have been extensively investigated in theory. However, in contrast to their 1D counterparts, the fundamental correlation of conformation with the size, bending rigidity, and surface interaction still remains unsolved in both experiments and theory. Here we report the scaling relations of 2D macromolecules by using single-layer graphene oxide as the model, underpinning a general framework to understand and measure their thermodynamic and rheological behaviors. Using Ubbelohde capillary rheology, we experimentally determined the Flory-type and Mark−Houwink−Sakurada scaling rules in the self-avoiding, good-solvent regime through the critical overlapping concentration ($C^* \sim L^{-0.87}$, L is the lateral size) and intrinsic viscosity ($[\eta] \sim M^{\alpha}$, $\alpha = 0.33$, M is the molecular weight). The measured exponent $\gamma = 0.87$ is well located between self-avoiding (4/5) and rigid (1) limit, indicating a nearly flat conformation and semiflexible nature, and $\alpha = 0.33$ differs from the value of polymers (0.5−0.8), signaling the dimensional constraint. The discussion of conformational size-scaling relations is complemented by dissipative particle dynamics simulations, which clarify the effects of size and bending resistance of 2D macromolecules as well as the solvent that tunes their surface interaction, resulting in conformation transitions among nearly flat, folded, and crumpled phases.

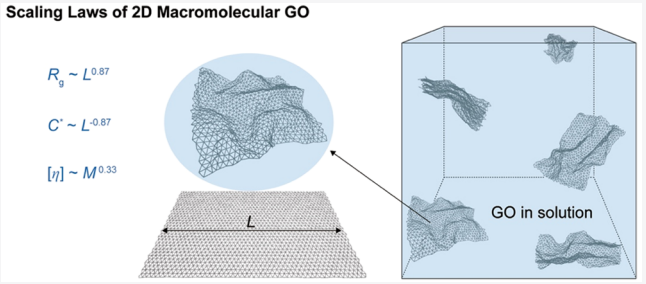

INTRODUCTION

Macromolecules with covalently bonded molecular units in diverse geometries have varying topologies, including 1D chains, 3D dendrimers, and the flourishing 2D macromolecules.[1−4] Graphene and 2D macromolecules in general,[5,6] both natural and synthetic, add a new dimension in the development of materials and devices for applications in electronics,[7] optoelectronics,[8] structural and functional materials,[9−13] energy,[14] and biology[15] which are usually realized through solution processing. Understanding the thermodynamic and rheological behaviors of 2D macromolecules in solution is thus of fundamental importance, especially for assessing their conformation and designing properties of materials and devices.

1D polymers, although featuring unimaginable chemical complexity, demonstrate remarkably simple yet general scaling laws that govern their statistical and dynamical behaviors.[1,2] Freely jointed Kuhn segments of polymeric chains conform to the random walk model, and the radius of gyration (R_g) scales with the contour length of a chain (L) as $R_g \sim L^{\gamma} \sim M^{\gamma} \sim N^{\gamma}$ (M is the molecular weight and N is the degree of polymerization). The universal exponent γ is deduced for 1D polymers as 0.5 in the theta solvent, 0.6 in good solvents, and 0.5 in melts.[1] These fundamental scaling relations have been justified in experiments and lay the ground for polymer science and technology. For example, the intrinsic viscosity $[\eta]$ for polymer solutions, defined as the ratio between the specific viscosity and the polymer concentration at the dilute limit, is correlated to the molecular weight of soluble polymers (M) through the Mark−Houwink−Sakurada (MHS) equation $[\eta] = KM^{\alpha}$,[2] which becomes a standard method to measure M.

For 2D manifolds, studies on the conformational behaviors of polymerized membranes of both fluid and solid have been pursued in theory over the past few decades.[16−20] Geometrical consideration suggests the Flory-type scaling relation $R_g \propto L^{\gamma}$ with $\gamma = 2/3$ and 1 for the compact and rigid limits.[20] The self-penetrable phantom model of tethered membranes displays a scaling relation of $R_g \sim (\ln L)^{1/2}$.[18] Generalization of the Flory relation for polymers to membranes yields a $\gamma = (2 + D^*)/(2 +$

Received: June 18, 2020
Revised: November 4, 2020
Published: November 18, 2020

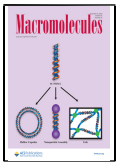

https://dx.doi.org/10.1021/acs.macromol.0c01425
Macromolecules 2020, 53, 10421−10430

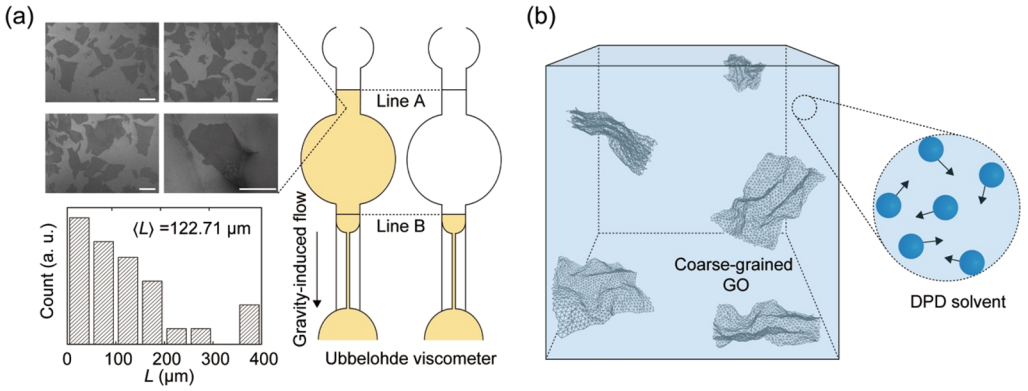

Figure 1. (a) SEM images of GO sheets in the solution, GO size distribution, and the schematic of measuring the viscosity of GO solution with a Ubbelohde viscometer. The scale bars are 100 μm. (b) GO solution modeled as sheets of covalently coarse-grained beads solved by DPD particles for the solvent.

d) = 4/5 for self-avoiding tethered membrane in a good solvent without bending resistance, where $D^* = 2$ and $d = 3$ are the dimensions of the manifold and space, respectively.[16] Including the bending resistance of membranes and/or surface interactions (e.g., adhesion and repulsion), simulations suggest scaling behaviors with γ varying between the compact and rigid limits.[19,21,22] The wide spectrum of these theoretical predictions implies the rich physics of conformational scaling behaviors of 2D macromolecules in correlation with their size, rigidity, and surface interactions.

In contrast, the experimental exploration in this scenario is quite limited.[23−28] Static light scattering (SLS) measurements extracted scaling relations of graphite oxide platelets with a specific lateral size (~5 μm) in solvents by measuring the fractal dimension (d_f = 2.5) and concluded $\gamma = 2/d_f$ = 0.8.[20,24,26] However, the conclusion has been questioned by the low accuracy of SLS techniques as well as the wide distribution of lateral sizes and polydispersity in the thickness.[27] The Flory exponent determined thus fails to rule out the mixing effects of soft and rigid sheets. Moreover, crumpled phases of 2D polymers predicted in theory have not been identified for graphite oxide in freeze-fracture electron microscopy[27] and graphene oxide (GO) in optical microscopy[29] in solution. To date, the conformational scaling behaviors of 2D macromolecules still remain as an open question, which should be addressed by using samples with well-defined thickness and reliable experiments beyond SLS.

Molecular simulations have been shown as a powerful method to explore conformational behaviors for 2D macromolecules.[18,19,21,22,30,31] The dissipative particle dynamics (DPD) takes an explicit solvent approach that can include the solid−liquid interfacial interaction and hydrodynamic effects, making it an efficient mesoscale method to study the systems of complex fluids.[32,33] In simulating polymer solutions, the soft, repulsive force in standard DPD alone fails to reproduce the overlapping of polymer segments, which should be supplied with additional conservative forces. Symeonidis et al.[34] used DPD simulations to study the scaling law of 1D polymer chains with different forms of conservative forces such as Lennard-Jones, Hookean−Fraenkel, finitely extensive nonlinear elastic models, and worm-like chains. The DPD model was also updated to model shape evolution of the human red blood cells (RBCs) and effective viscosity in shear flow, where the RBCs were coarse-grained into a closed surface with a hexagonal lattice surrounded by DPD particles of flows.[35,36] In this work, DPD simulations were performed to study the conformational phase behaviors GO in solvent and the effective viscosity.

Here, we perform Ubbelohde capillary rheology measurements to directly determine the conformation-size scaling laws of 2D macromolecules in good solvents by using single-layer GO as the model. For the first time, we directly extract the scaling relation between R_g and the contour length L of monolayer GO by rheological methods. We show that GO behaves self-avoiding, nearly-flat membranes in good solvents, and the Flory exponent γ = 0.87 evidently deviates from predictions for the compact and rigid surface limits. The generalized Flory exponent is verified by the MHS relation, with an exponent α = 0.33 which is distinct in comparison with that for 1D polymers ($0.5 < \alpha < 0.8$),[2] as a result of the dimensional constraint. Beyond these experimental evidences, we perform DPD simulations to clarify the effects of size, rigidity, and surface interaction of 2D macromolecules, which identify the microscopic origins of measured scaling relations. Finally, a general theoretical framework is developed to characterize their thermodynamic and rheological behaviors, offering a systematic guidance for the design and engineering of their applications in advanced materials and devices.

EXPERIMENTAL SECTION

Preparation of Single-Layer GO. We prepared GO samples with different average lateral sizes by using the modified Hummers method following our established procedures.[37] Typically, natural graphite flakes (different crystal sizes, 5 g) were added into a 500 mL flask with 98% sulfuric acid (150 mL), and the mixture was kept at room temperature and stirred at a speed of 300 rpm/min. Potassium permanganate (20 g) was then slowly added into the flask under continuous stirring where the temperature of mixture was lower than 5 °C. After the reaction was complete, the mixture was diluted with 2 L of water, followed by dropwise addition of 30% H_2O_2 until no bubbles were generated. The mixture was repeatedly washed with water by using the centrifugation washing method. Finally, aqueous GO solutions with different GO sizes were obtained, and the average lateral size of each GO sample was calculated based on a collection of over 100 sheets. We replaced water by *N*,*N*-dimethylformamide (DMF) via a repeating centrifugation method for five times to obtain GO/DMF dispersions with the same concentration. For GO solutions with mixed solvents, ethyl acetate (EA) and acetone were directly added into the DMF solution and sufficiently mixed to a homogeneous solution.

Ubbelohde Capillary Rheology. We measured the concentration of GO aqueous solution by freeze-drying and then diluted the

https://dx.doi.org/10.1021/acs.macromol.0c01425
Macromolecules 2020, 53, 10421−10430

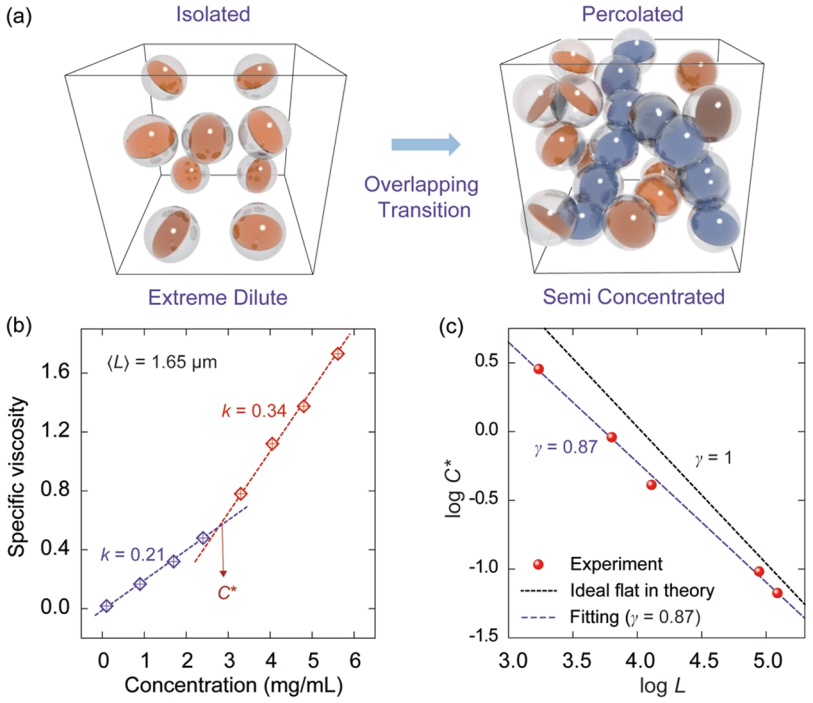

Figure 2. (a) Illustration of the overlapping transition of GO from extreme dilute to semiconcentrated DMF solutions. (b) Specific viscosity plotted as a function of GO concentration with an average lateral size of 1.65 μm. (c) Concentration at overlapping transition plotted as a function of the average size of GO sheets (for experimental details see the Supporting Information).

aqueous, DMF solution, or the mixture to eight concentrations before measuring the viscosity with a Ubbelohde viscometer (Figure 1a). To improve the accuracy of measurement, the solution was prepared by volumetric flask, and measurement was conducted instantly after preparation. Each data point was repeated for at least three times until the range of three sequential measurements was within 0.2 s at a constant temperature of 25 °C. Normally, the measured time t, defined as the time for GO solution flow between line A and line B in Figure 1a, by using a Ubbelohde viscometer in this experiment was in the range 70−350 s. The relative viscosity is calculated as $\eta_r = \eta_{solution}/\eta_{solvent} = t_{solution}/t_{solvent}$, and thus the specific viscosity is $\eta_{sp} = (\eta_{solution} - \eta_{solvent})/\eta_{solvent} = t_{solution}/t_{solvent} - 1$.

SIMULATION METHODS

Dissipative Particle Dynamics Models for Solvents and GO. DPD simulations are implemented to explore the dynamic behaviors of dilute GO solution, where both the GO sheets and solvent are modeled by using coarse-grained beads.[32,38,39] The coarse-grained model for GO sheets is constructed through a hexagonal lattice as shown in Figure 1b. The bonds are modeled as linear elastic springs, and a pair of triangular facets sharing a common edge is modeled as a dihedral. Atoms in the GO sheet are grouped into beads with equal masses. The bonding interaction between beads is modeled through a stretching energy term $E_s = k_s(r - r_0)^2/2$ with a stiffness $k_s = \frac{\sqrt{3}}{2}Yt$, where r_0 is the equilibrium interbead distance, and Yt, the product of Young's modulus and thickness, is the 2D tensile stiffness of the GO sheet.[31] The bending resistance of a GO sheet is modeled by a dihedral term $E_b = k_d(1 - \mathbf{n}_i\mathbf{n}_j)$ with a stiffness $k_d = \frac{2}{\sqrt{3}}D$, where $\mathbf{n}_i$ and $\mathbf{n}_j$ are the unit normal vectors of triangles i and j sharing a common edge and D is the bending stiffness of GO. This dihedral term is equivalently expressed by using a harmonic potential of dihedral angle φ as $E_b = k_d(1 + \cos\varphi)$. Here we use D instead of YI to avoid the ambiguity in the definition of the thickness t for single-atom-thick sheets. The bending stiffness of GO is reported to be ~1 k_BT at room temperature,[40] and thus the bending stiffness is chosen within 0−10 k_BT. The implementation of adhesion between GO membranes follows previous studies,[34,35] where the pairwise interaction between nonbonding beads (beads not interacting through the bond stretch and dihedral terms) in GO sheets is added to the DPD force field, in the form of Lennard-Jones 12-6 potential $E_{L\text{-}J} = 4\varepsilon[(\sigma/r)^{12} - (\sigma/r)^6]$, with a cut-off distance of 2.5σ. The details of DPD method and the parameters for the GO sheets can be found in the Supporting Information.

DPD Simulation Setup. The DPD simulations are performed by using the large-scale atomic/molecular massively parallel simulator (LAMMPS).[41] The size of the supercell is 30R_c containing ~81000 DPD beads, and the lateral length of the GO sheets is set to range from 7R_c to 35R_c, where R_c is the DPD length unit (Table S1). The GO solutions are relaxed over 2.0 × 10^6 timesteps with k_BT = 1, corresponding to 300 K. After equilibration, the shear viscosity is calculated by using the Green−Kubo formalism through the autocorrelation function of pressure tensor (PACF) $\mathbf{P}$.[42] The intrinsic viscosity of GO is defined as $[\eta] = \lim_{c\to 0}\frac{\eta - \eta_0}{c\eta_0} = \lim_{c\to 0} f(c)$, where η_0 is the viscosity measured at a concentration of c = 0. To quantitatively describe the morphologies of GO sheets, the radius of gyration tensor $\mathbf{S}$, the relative shape anisotropy,[43] and the solvent accessible surface area (SASA)[44] are calculated (Supporting Information). The hydrodynamic radius, R_h, is computed via Stokes−Einstein relations, with the translational and rotational diffusion coefficients, D_t and D_r, which are calculated by the mean-square displacement (MSD) and angular mean-square displacement (AMSD), respectively.[45,46]

https://dx.doi.org/10.1021/acs.macromol.0c01425
Macromolecules 2020, 53, 10421−10430

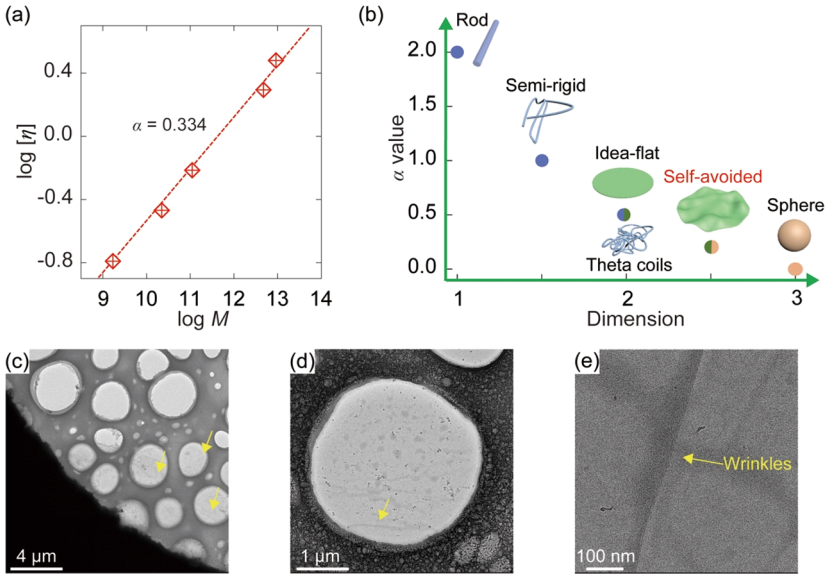

Figure 3. (a) Intrinsic viscosity of GO−DMF solution plotted as a function of the molecular weight of GO sheets, from which the MHS relation is extracted (see experimental details in the Supporting Information). (b) Conformational phases of 2D macromolecules identified by the exponent in the MHS relation. (c−e) Cryo-TEM images of GO sheets embedded in amorphous ice. Wrinkles in the GO sheets are annotated by the arrow.

RESULTS AND DISCUSSION

By choosing the size of raw graphite crystals, the produced GO sheets had a series of average lateral size of $\langle L\rangle$ = 1.65, 6.34, 12.91, 88.24, and 122.71 μm (Figures S1−S5, Supporting Information). A uniform thickness of ∼1 nm of GO sheets deposited from the DMF solution under atomic force microscopy (AFM) suggests their monolayer nature in solutions.[37] Selected area electron diffraction (SAED) under transmission electron microscopy (TEM) reveals that GO partly retains the sp^2 lattice of graphene even after oxidation (Figure S6). These single-layer GO sheets thus become an ideal model to examine the conformational scaling relations of 2D macromolecules.

The conformation of 2D macromolecules defines their rheological behaviors,[20,47−49] offering a reliable way to extract their average conformational information through simple rheology tests beyond the SLS method with low accuracy.[24,26] The first deduction is the existence of a critical overlap concentration (C^*) which corresponds to the percolation threshold of GO monolayers in solution as a continuous network forms or a local orientation order emerges (Figure 2a). In good solvents, 2D macromolecules retain the nearly flat conformation and can be considered as disks with a diameter of $2\sqrt{2}R_g$. Both theories and numerical simulations conclude that C^* scales linearly with $1/R_g$ by neglecting the change of thickness at high aspect ratios.[50,51] Therefore, we have a scaling relation for C^*

$$C^* \propto {R_g}^{-1} \propto L^{-\gamma} \tag{1}$$

For nearly-flat membranes, the viscous flow of their dilute solution can be simplified to the diffusion of spheres by considering their rotation. The size of spheres measured by the lateral size of the membrane is $2\sqrt{2}R_g$ following the spirit of Zimm's single-chain-drop assumption for 1D polymers.[2,16] The intrinsic viscosity $[\eta]$ is determined by the Einstein−Stokes relation[2] as

$$[\eta] = \lim_{c\to 0}\frac{\eta-\eta_0}{\eta_0 c} = 2.5\frac{N_A V_e}{M} \tag{2}$$

Here c is the concentration, the prefactor of 2.5 is the Einstein parameter for spheres, N_A is Avogadro's number, and $V_e = \frac{\pi {R_g}^3}{6}$ is the equivalent hydrodynamic volume in the Zimm assumption. We then have

$$[\eta] = \frac{5\pi N_A {R_g}^3}{12\rho L^2} = K\frac{L^{3\gamma}}{L^2} = KL^{3\gamma-2} \tag{3}$$

where K is another prefactor and ρ is the areal density of rigid 2D macromolecules ($M = \rho L^2$). A scaling law relating $[\eta]$ with M is thus deduced as

$$[\eta] \propto L^{3\gamma-2} \propto M^{(3\gamma-2)/2} = M^{\alpha} \tag{4}$$

For self-avoiding, tethered macromolecules with a theoretically predicted exponent of γ = 4/5, $[\eta] \propto M^{1/5}$.

We use the Ubbelohde capillary rheology to determine the scaling relations of single-layer GO solutions. The specific viscosity $\eta_{sp} = \eta_{solution}/\eta_{solvent} - 1$ of DMF solutions of GO with $\langle L\rangle$ of 1.65 μm increases with c, experiencing a transition at the percolation threshold $C^* = 2.8 \times 10^{-3}$ wt % (Figure 2b). η_{sp} scales linearly with c as $0.20c$ and $0.34c$ before and after the transition, respectively. This transition is universal for solutions with different lateral sizes of GO (Figure S7), from which in eq 1 we conclude $C^* \sim L^{-0.87}$ (Figure 2c). The exponent $\gamma = 0.87 \pm 0.03$ thus measured is far below the limit 1 for rigid surfaces but higher than the value γ = 4/5 for self-avoiding, tethered membranes,[17,18,20] suggesting that GO monolayers maintain a nearly planar conformation with undulation in a good solvent. We use the average size of GO sheets to estimate the exponents. However, the distribution of lateral sizes may lead to statistical effects. To address this issue, we prepared samples with average sizes $\langle L\rangle$ spanning over 2 orders of magnitude. The deviation in size for three representative sets of samples ($\langle L\rangle$ = 1.65, 12.91, and 122.7 μm) is much smaller than the size contrast between them (Figures S1, S3, and S5). The

https://dx.doi.org/10.1021/acs.macromol.0c01425
Macromolecules 2020, 53, 10421−10430

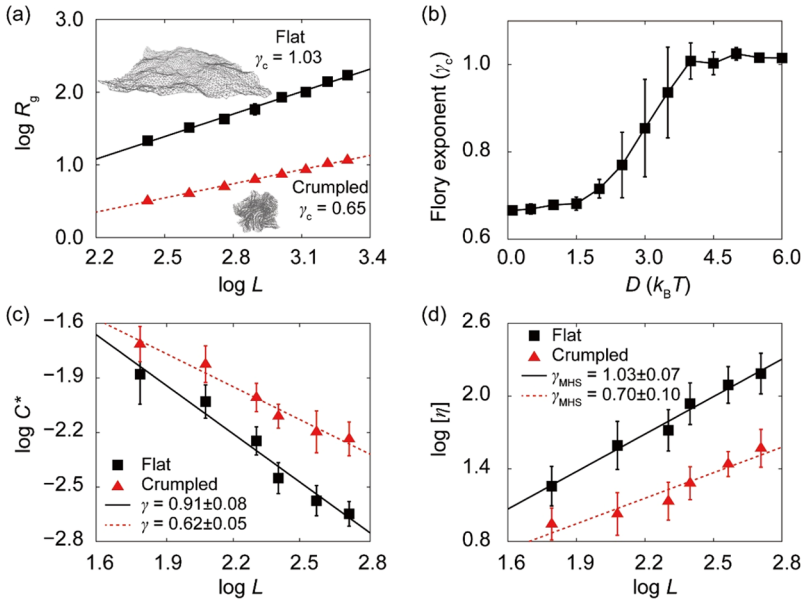

Figure 4. (a) Radius of gyration R_g measured for GO sheets as a function of the lateral size, L. The results are obtained from DPD simulations and fitted into a conformational scaling relation $R_g \sim L^{\gamma}$ for both flat and crumpled GO correspond to bending rigidity, $D = 6\ k_BT$ and $1\ k_BT$, respectively. The insets are the typical flat and crumpled conformations. (b) The exponent γ_c plotted as a function of bending rigidity, D. (c) The critical concentration C^* plotted as a function of L for both flat ($D = 6\ k_BT$) and crumpled ($D = 1\ k_BT$) GO sheets. (d) The intrinsic viscosity $[\eta]$ plotted as a function of L for both flat ($D = 6\ k_BT$) and crumpled ($D = 1\ k_BT$) GO sheets.

statistical effects can thus be excluded in the scaling relations obtained using the average size, which can reasonably capture the 2D macromolecular behaviors of GO. The scaling relation $C^* \sim L^{-0.87}$ can be used as a standard reference to measure the average size of GO in DMF through simple rheology tests. This constrained scaling behavior between the theoretical limits of disks and sphere (Figure 3b) demonstrates the semiflexible nature of GO sheets.

We then measured $[\eta]$ of GO DMF solutions and revealed a MHS relation as

$$[\eta] = KM^{0.33\pm0.02} \quad (5)$$

Here the molecular weight M is calculated by number-average as detailed in Figure S8. Combined with eq 4, we conclude $\gamma_{MHS} = 0.89 \pm 0.017$, which aligns well with the value $\gamma = 0.87$ extracted from the C^* measurements (Figure 2c). The MHS rule is valid for weight-average and Z-average molecular masses as well (Figure S8), yielding exponents of $\alpha = 0.282$ and 0.277, respectively, which further suggests a minor effect of the lateral size distribution.

Previous SLS studies suggested a Flory exponent of $\gamma \sim 0.8$ for graphite oxide colloids with an average size of $\langle L \rangle = \sim 5$ μm,[24,26] which seems to perfectly meet the theoretical prediction for self-avoiding surfaces.[17,18,20] Our SLS results for GO solutions with relatively larger size ($\langle L \rangle = 122.7$ μm) show $d_f = \sim 2.7$ and $\gamma \sim 0.74$ (Figure S9), signaling a size effect that was not considered in previous studies where the Flory exponent is determined from the fractal dimension.[24,26] Moreover, Spector et al. also raised concerns about the accuracy of SLS that may not be able to discriminate the planar and crumpled phases.[27] In comparison, our rheological tests offer a more reliable method to measure the conformational behaviors because of the improved accuracy and explicit account for size scaling. Our cryo-TEM characterization further validates the nearly planar conformation of GO in good solvents, where wrinkles are present but not crumpled (Figure 3c–e). This conclusion agrees with the electron microscopy observation and many recent experiment results.[5,9,27,37]

The scaling relations (Figures 2c and 3a) clarify the ambiguity in thermodynamic and rheological behaviors of GO in solution, which can be extended to 2D macromolecules in general.[24,26−29] To explore the effects of the size and flexibility of 2D sheets, we perform DPD simulations as detailed in the Simulation Methods section and Supporting Information. The solvent is modeled by using beads interacting through a DPD force field with conservative, dissipative, and random forces included, while GO are discretized into a hexagonal lattice of coarse-grained beads, where bond-stretch and dihedral energy terms are included to model the in-plane elasticity and out-of-plane bending rigidity, respectively. The GO−solvent interaction is also modeled by using the DPD force field, while an additional pairwise interaction in the Lennard-Jones form is added between the nonbonding beads in GO to account for the adhesion. GO conformation in the dilute limit is defined by the competition between its bending resistance and thermal fluctuation. By varying their bending rigidity D, the sheets are identified from the flat to the compactly crumpled in our simulations. The conformational scaling relation $R_g \sim L^{\gamma}$ extracted from DPD simulations (Figure 4a) concludes $\gamma_c = 1.03 \pm 0.03$ for the flat sheet (approaching the rigid limit of 1) and $\gamma_c = 0.65 \pm 0.01$ for the crumpled ones (approaching the compact limit of 2/3).[20] Here we use γ_c for the Flory exponent derived directly from the conformation scaling relation, which differs from γ that is determined from the critical concentration of overlapping transition, C^*, and γ_{MHS} from the MHS rule. We identify a critical bending rigidity of $\sim 3k_BT$ that discriminates the planar and compactly crumpled phases (Figure 4b).[31,40] The bending rigidity of pristine graphene is $\sim 40\ k_BT$,[52−54] which is high enough to be flat according to our DPD results if it can be solved in solvents. However, while oxidized, the bending

https://dx.doi.org/10.1021/acs.macromol.0c01425
Macromolecules 2020, 53, 10421−10430

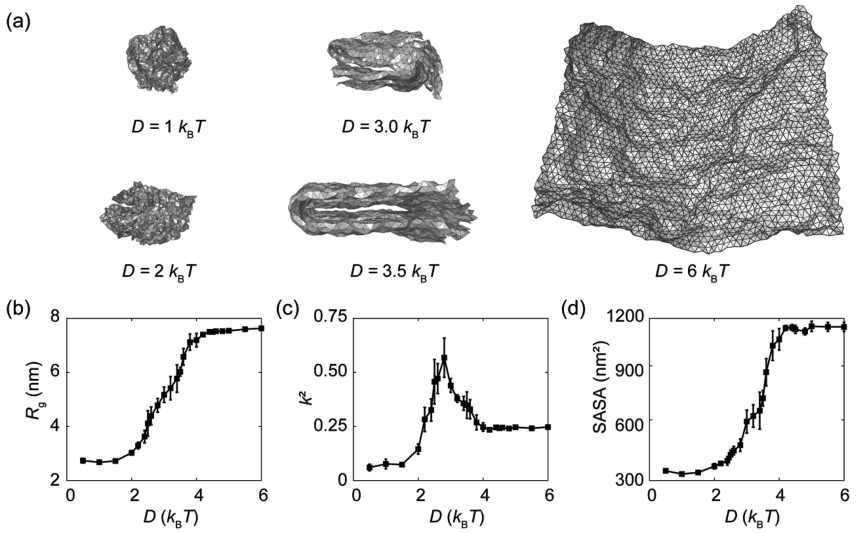

Figure 5. (a) Conformational evolution of GO sheets with different bending rigidities, D. (b–d) Conformational measures including (b) the radius of gyration, R_g, (c) the relative shape anisotropy, κ^2, and (d) the solvent accessible surface area (SASA) plotted as functions of D. The size of square GO sheets in the simulations is L = 22.6 nm.

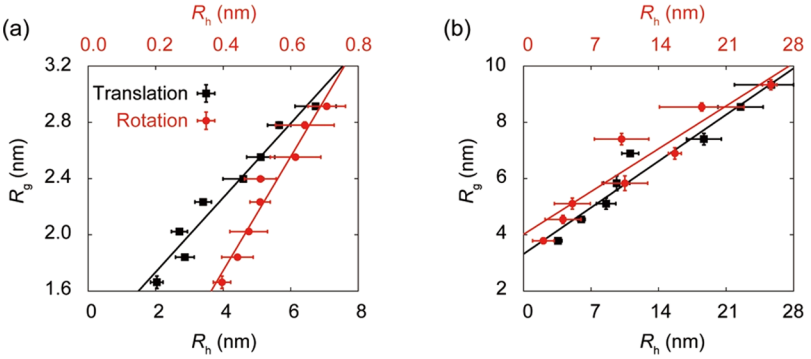

Figure 6. Relationship between hydrodynamic radius R_h and the radius of gyration R_g calculated for GO sheets in (a) crumpled (D = 1 k_BT) and (b) flat conformations (D = 6 k_BT). The values of R_h are calculated from both translational and rotational diffusion coefficients.

rigidity of GO can be significantly modified by the degree of oxidation, types of functional groups,[55] and defects.[56] Experimental studies show that the value of D is ∼1 k_BT,[40] close to the marginal value between planar and crumpled phases. It is also interesting to note that this critical value of D is close to that of lipid bilayers (a few k_BT),[57,58] and the study of GO solutions here could offer insights into biological membranes.

In addition to R_g, the morphology of GO in solution is also measured by the relative shape anisotropy κ^2 and solvent accessible surface area (SASA). The shape descriptor κ^2 measures symmetry and dimensionality of a macromolecule,[43,59] ranging from 0 (sphere) to 1 (line). The SASA of 2D macromolecules is calculated by considering the DPD particles as spheres.[44,60] Our simulation results show that R_g and SASA exhibit a similar dependence on D as γ_c does, while κ^2 demonstrates a peak at the transition point of D = ∼3k_BT (Figure 5). As D increases, 2D macromolecules evolve from isotropic crumples (D = 1, 2 k_BT, κ^2 close to 0) to tubular or folded configurations with notable anisotropy (D = 3.0, 3.5 k_BT) and to flat conformation (D = 6 k_BT) with κ^2 approaching the planar limit of 0.25 (Figure 5c). These results validate again the Flory exponent γ = ∼0.87 we measured experimentally (Figure 4b), between the compact (2/3), self-avoiding (4/5), and rigid limits (1).

The viscosity of 2D macromolecule solution is studied through the Green–Kubo formalism using the pressure–pressure autocorrelation function in DPD simulations.[42] For rigid sheets, the relationship between the hydrodynamic radius R_h and R_g is analytically proved to be linear.[30,61] Our results suggest a linear relation between R_g and R_h for both crumpled and flat conformations (calculated from the translational and rotational diffusion coefficients, Figure 6). The well-resolved R_g–R_h relation allows us to adopt eqs 1–3 to explore the rheological behaviors of 2D macromolecules. We find that C^* decreases with L, where the scaling exponent is calculated as γ = 0.91 ± 0.08 and 0.62 ± 0.05 for flat and crumpled conformations, respectively (Figure 4c). The scaling exponent in $[\eta]$ for the MHS relation is predicted as α = 0.54 (γ_{MHS} = 1.03 ± 0.07) for flat (D = 6 k_BT) and α = 0.05 (γ_{MHS} = 0.70 ± 0.10) for crumpled conformations (Figure 4d), in consistency with the values of γ_c and γ extracted from DPD simulations using the conformational scaling relation and critical overlapping transition, respectively. Our experimental results are well located within this theoretical range, which implies that GO sheets have a moderate bending rigidity in the solution.

Our discussion above excludes the effects of solvent, where surface adhesion and electrostatic repulsion between GO can notably modify their behaviors.[27] DMF is a good solvent for GO as evidenced in solution processing of GO, where liquid

https://dx.doi.org/10.1021/acs.macromol.0c01425
Macromolecules 2020, 53, 10421–10430

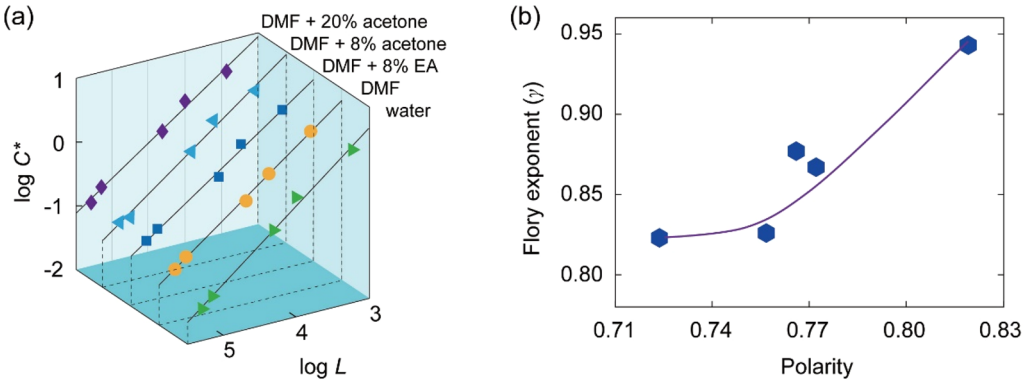

Figure 7. (a) Overlapping transition concentration of GOs with different sizes and types of solvents. (b) Measured Flory exponent from data in (a) plotted against the solvent polarity, from small to large values for DMF + 20% acetone, DMF + 8% acetone, DMF + 8% EA, DMF, and water.

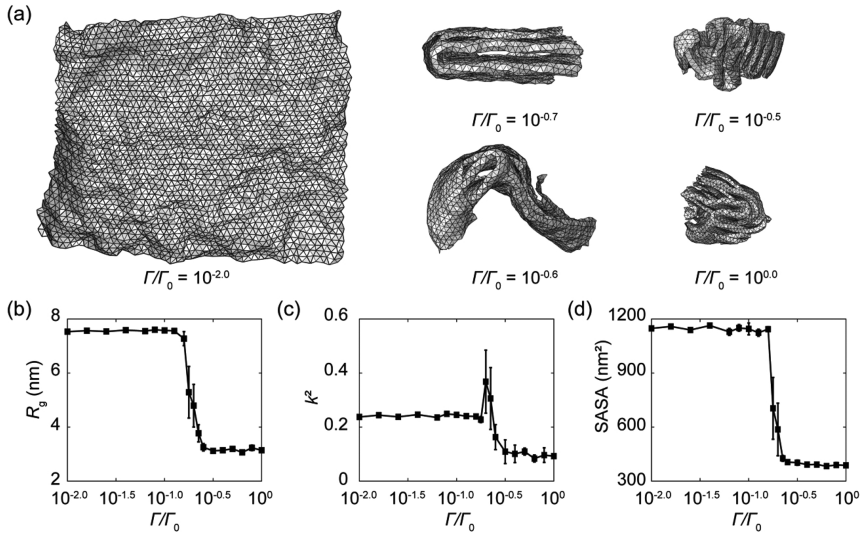

Figure 8. (a) Conformational evolution of GO sheets with different adhesion energy density measured in the surface interaction Γ/Γ_0. Here Γ_0 is the adhesion energy density of GO sheets in vacuum. (b–d) Conformational measurements including (b) the radius of gyration, R_g, (c) the relative shape anisotropy, κ^2, and (d) the solvent accessible surface area (SASA), plotted as functions of Γ/Γ_0. The size of square GO sheets is L = 22.6 nm in the simulations, and the bending rigidity is $D = 5\ k_BT$.

crystal forms or planar conformations of GO are identified in DMF.[12,62] The use of DMF as a good solvent enables us to tune the polarity of the solvents by adding poor solvents for GO such as EA and acetone. We find that the Flory exponent γ increases with either the polarity of solvents (Figure 7) or solubility parameter (Figure S10). As the ratio of acetone increases to 20 vol %, γ decreases to 0.82, denoting a lateral shrinkage of GO sheets from the planar conformation in good solvents. A higher poor-solvent ratio leads to further shrinkage of GO sheets and brings severe inhomogeneity; as a result, the measurement of viscosity becomes unreliable as fluffy precipitation appears. In aqueous solution, we find $\gamma = 0.94 \pm 0.03$, which is notably higher than the value $\gamma = 0.87$ for DMF. This morphological change towards flat membranes in aqueous solution is possibly caused by the stronger electrostatic repulsion that stiffens the GO sheets.[63] The Flory scaling exponents of GO depend on their morphological conformation, which can be well tuned by the properties of GO sheets or the polarity of solvent. The exponents for compact crumples and flat sheets represent the lower and upper bounds for the rich spectrum of phases. However, as the morphology of phases such as nearly-flat membranes, scrolls, folds, crumples, and intermolecular complexes are not distinctly defined, one cannot assign unique scaling exponents to them. Our DPD simulations extend the parametric space in experimental studies, predicting the range of scaling exponents for different phases of GO. For example, by tuning the bending stiffness D of GO (Figures 5), we have $\gamma_c = \sim 0.67$ for compact crumples ($D = 1\ k_BT$), $\gamma_c = 0.70–0.92$ for nearly flat membranes or semicrumples, folds, and scrolls ($D = 2$, 3, and 3.5 k_BT), and $\gamma_c = \sim 1.0$ for flat sheets ($D = 6\ k_BT$).

As reported in ref 63, the reduction in electrostatic repulsion by increasing the DMF concentration helps GO sheets overcome the energy barrier for change from the flat to the scrolled morphology.[64] We prepare the GO/DMF solutions by replacing water in aqueous GO solution with DMF. The nearly flat conformation of GO identified in GO/DMF (Figure 1a) suggests that DMF is a good solvent. The surface adhesion from the van der Waals interaction, however, is weakened by DMF. To understand the solvent effects, we performed DPD simulations with different adhesion energy density (Γ) defined for GO sheets.[34,35] Because strong electrostatic repulsion prevents GO sheets from scrolling or crumpling transitions, which disagrees with our experimental observation, we focus our discussions on the flat-crumpling transition with a relatively weak electrostatic repulsion incorporated to the

https://dx.doi.org/10.1021/acs.macromol.0c01425
Macromolecules 2020, 53, 10421−10430

surface adhesion. The reference adhesion energy density is $\Gamma_0 = 0.31$ J/m^2 for graphene in the vacuum, and in solvent we have $\Gamma/\Gamma_0 < 1$ (Figure 8).[65] At low Γ values, GO sheets remain nearly flat for $D = 5\ k_BT$, which is larger than the critical value $D = \sim 3\ k_BT$ in the absence of surface adhesion. With enhanced surface adhesion, GO exhibits folding/tubular transitions and sequentially crumpling (Figure 8a). The morphological measures (R_g, κ^2, and SASA, Figures 8b−d) show that GO sheets remain crumpled for adhesion $\Gamma/\Gamma_0 > 10^{-0.5}$. Similar to the transition identified (Figure 8), the folding/tubular morphologies around the transition show high anisotropy, $\kappa^2 = \sim 0.4$. Combining these results with the experimental evidences in Figure 7b, we conclude that the increase of γ with the solvent polarity results from an effective reduction in the surface adhesion of GO. In highly polar solutions such as water, the negative charge density increases, and thus the free energy barrier of folding or crumpling is inaccessibly high compared with the thermal fluctuation,[64] which thus renders GO sheets with more planar conformation.

The conformational scaling laws of 2D macromolecules allow us to address practical issues in a versatile way as for the 1D polymers. For example, one can measure the molecular weight of 2D macromolecules from the MHS equation with a known scaling exponent. This exponent characterizes conformations that can be categorized into distinct phases of nearly flat membranes, scrolls, folds, crumples, and intermolecular complex, which have great impacts on the fabrication process of macroscopic assemblies such as fibers and membranes from solutions.[66,67] Compact, well-aligned, defect-free, large-sized GO sheets often lead to elevated mechanical properties and transport performance. Microstructural features of these assemblies such as pores, channels at wrinkles, and open spaces between the sheet edges also determine the permeability and selectivity of GO films.[68] The viscoelasticity of 2D macromolecules in solution is also an important issue that is related to applications such as 3D printing with GO solution.[69] However, conformational scaling relations for the storage and loss modulus (G' and G'') have not been well addressed in theory. In experiments, the measured viscoelastic moduli of GO solutions depends on the strain amplitude, loading frequency, and concentration.[70] A complete picture of the viscoelastic behaviors is out of the scope for the current work which is mainly focused on the dilute GO solution, where DPD simulations suggest that the viscous effect is dominant (Figure S11).

CONCLUSION

In summary, we experimentally determined the conformational scaling laws of 2D macromolecules by using single-layer GO as the model. Ubbelohde capillary rheology measurements show that GO in good solvents behaves as a self-avoiding, nearly flat membrane with out-of-plane fluctuations, featuring a generalized Flory exponent of $\gamma = 0.87$ and the MHS relation with an exponent of $\alpha = 0.33$. A general description of thermodynamic and rheological behaviors of 2D macromolecules is constructed based on DPD simulations. The Flory exponent identified spans the whole range from the compact (2/3) to the rigid (1) limit, demonstrating the crucial effects of the mechanical and surface properties as well as the solvents. The conformational scaling relations reported in this paper extend the framework of polymer physics to the 2D manifold, offering principles that can be used in the understanding and control of their assembly and processing in solution toward applications.

ASSOCIATED CONTENT

Supporting Information

The Supporting Information is available free of charge at https://pubs.acs.org/doi/10.1021/acs.macromol.0c01425.

Experimental details, simulation details, viscoelastic scaling relations of GO solutions, supplemental tables, figures, and captions, supplemental references (PDF)

AUTHOR INFORMATION

Corresponding Authors

Zhen Xu − *MOE Key Laboratory of Macromolecular Synthesis and Functionalization, Department of Polymer Science and Engineering, Key Laboratory of Adsorption and Separation Materials & Technologies of Zhejiang Province, Zhejiang University, Hangzhou 310027, P. R. China;* orcid.org/0000-0001-9282-9753; Email: zhenxu@zju.edu.cn

Zhiping Xu − *Applied Mechanics Laboratory, Department of Engineering Mechanics and Center for Nano and Micro Mechanics, Tsinghua University, Beijing 100084, P. R. China;* orcid.org/0000-0002-2833-1966; Email: xuzp@tsinghua.edu.cn

Authors

Peng Li − *MOE Key Laboratory of Macromolecular Synthesis and Functionalization, Department of Polymer Science and Engineering, Key Laboratory of Adsorption and Separation Materials & Technologies of Zhejiang Province, Zhejiang University, Hangzhou 310027, P. R. China*

Shijun Wang − *Applied Mechanics Laboratory, Department of Engineering Mechanics and Center for Nano and Micro Mechanics, Tsinghua University, Beijing 100084, P. R. China;* orcid.org/0000-0002-5654-8118

Fanxu Meng − *MOE Key Laboratory of Macromolecular Synthesis and Functionalization, Department of Polymer Science and Engineering, Key Laboratory of Adsorption and Separation Materials & Technologies of Zhejiang Province, Zhejiang University, Hangzhou 310027, P. R. China*

Ya Wang − *MOE Key Laboratory of Macromolecular Synthesis and Functionalization, Department of Polymer Science and Engineering, Key Laboratory of Adsorption and Separation Materials & Technologies of Zhejiang Province, Zhejiang University, Hangzhou 310027, P. R. China*

Fan Guo − *MOE Key Laboratory of Macromolecular Synthesis and Functionalization, Department of Polymer Science and Engineering, Key Laboratory of Adsorption and Separation Materials & Technologies of Zhejiang Province, Zhejiang University, Hangzhou 310027, P. R. China*

Sangeetha Rajendran − *MOE Key Laboratory of Macromolecular Synthesis and Functionalization, Department of Polymer Science and Engineering, Key Laboratory of Adsorption and Separation Materials & Technologies of Zhejiang Province, Zhejiang University, Hangzhou 310027, P. R. China*

Chao Gao − *MOE Key Laboratory of Macromolecular Synthesis and Functionalization, Department of Polymer Science and Engineering, Key Laboratory of Adsorption and Separation Materials & Technologies of Zhejiang Province, Zhejiang University, Hangzhou 310027, P. R. China;* orcid.org/0000-0002-3893-7224

Complete contact information is available at: https://pubs.acs.org/10.1021/acs.macromol.0c01425

https://dx.doi.org/10.1021/acs.macromol.0c01425
Macromolecules 2020, 53, 10421−10430

Author Contributions

P.L., S.W., and F.M. contributed equally to this work.

Notes

The authors declare no competing financial interest.

■ ACKNOWLEDGMENTS

We thank the support from the National Natural Science Foundation of China (Nos. 51973191, 51703194, 51533008, 51603183, 51803177, 21805242, 5197030056, and 11825203), the National Key R&D Program of China (No. 2016YFA0200200), the Hundred Talents Program of Zhejiang University (188020*194231701/113), the Key Research and Development Plan of Zhejiang Province (2018C01049), and the Fundamental Research Funds for the Central Universities (Nos. 2017QNA4036 and K20200060).

■ REFERENCES

(1) De Gennes, P. G. *Scaling Concepts in Polymer Physics*; Cornell University Press: Ithaca, NY, 1979.
(2) Doi, M.; Edwards, S. F. *The Theory of Polymer Dynamics*; Oxford University Press: New York, 1986.
(3) Schluter, A. D.; Payamyar, P.; Ottinger, H. C. How the world changes by going from one- to two-dimensional polymers in solution. *Macromol. Rapid Commun.* **2016**, *37*, 1638.
(4) Payamyar, P.; King, B. T.; Ottinger, H. C.; Schluter, A. D. Two-dimensional polymers: concepts and perspectives. *Chem. Commun.* **2016**, *52*, 18.
(5) Xu, M.; Liang, T.; Shi, M.; Chen, H. Graphene-like two-dimensional materials. *Chem. Rev.* **2013**, *113*, 3766.
(6) Servalli, M.; Schlüter, A. D. Synthetic two-dimensional polymers. *Annu. Rev. Mater. Res.* **2017**, *47*, 361.
(7) Torrisi, F.; Hasan, T.; Wu, W.; Sun, Z.; Lombardo, A.; Kulmala, T. S.; Hsieh, G. W.; Jung, S.; Bonaccorso, F.; Paul, P. J.; Chu, D.; Ferrari, A. C. Inkjet-printed graphene electronics. *ACS Nano* **2012**, *6*, 2992.
(8) Bonaccorso, F.; Sun, Z.; Hasan, T.; Ferrari, A. C. Graphene photonics and optoelectronics. *Nat. Photonics* **2010**, *4*, 611.
(9) Xu, Z.; Gao, C. Graphene chiral liquid crystals and macroscopic assembled fibres. *Nat. Commun.* **2011**, *2*, 571.
(10) Xiao, Y.; Xu, Z.; Liu, Y.; Peng, L.; Xi, J.; Fang, B.; Guo, F.; Li, P.; Gao, C. Sheet collapsing approach for rubber-like graphene papers. *ACS Nano* **2017**, *11*, 8092.
(11) Guo, F.; Zheng, X.; Liang, C.; Jiang, Y.; Xu, Z.; Jiao, Z.; Liu, Y.; Wang, H.; Sun, H.; Ma, L.; Gao, W.; Greiner, A.; Agarwal, S.; Gao, C. Millisecond response of shape memory polymer nanocomposite aerogel powered by stretchable graphene framework. *ACS Nano* **2019**, *13*, 5549.
(12) Li, P.; Liu, Y.; Shi, S.; Xu, Z.; Ma, W.; Wang, Z.; Liu, S.; Gao, C. Highly crystalline graphene fibers with superior strength and conductivities by plasticization spinning. *Adv. Funct. Mater.* **2020**, 2006584.
(13) Li, P.; Yang, M.; Liu, Y.; Qin, H.; Liu, J.; Xu, Z.; Liu, Y.; Meng, F.; Lin, J.; Wang, F.; Gao, C. Continuous crystalline graphene papers with gigapascal strength by intercalation modulated plasticization. *Nat. Commun.* **2020**, *11*, 2645.
(14) Xiao, L.; Damien, J.; Luo, J.; Jang, H. D.; Huang, J.; He, Z. Crumpled graphene particles for microbial fuel cell electrodes. *J. Power Sources* **2012**, *208*, 187.
(15) Liu, Y.; Dong, X.; Chen, P. Biological and chemical sensors based on graphene materials. *Chem. Soc. Rev.* **2012**, *41*, 2283.
(16) Cates, M. E. Statics and dynamics of polymeric fractals. *Phys. Rev. Lett.* **1984**, *53*, 926.
(17) Kantor, Y.; Kardar, M.; Nelson, D. R. Statistical mechanics of tethered surfaces. *Phys. Rev. Lett.* **1986**, *57*, 791.
(18) Kantor, Y.; Kardar, M.; Nelson, D. R. Tethered surfaces: Statics and dynamics. *Phys. Rev. A* **1987**, *35*, 3056.
(19) Plischke, M.; Boal, D. Absence of a crumpling transition in strongly self-avoiding tethered membranes. *Phys. Rev. A* **1988**, *38*, 4943.
(20) Nelson, D.; Piran, T.; Weinberg, S. *Statistical Mechanics of Membranes and Surfaces*; World Scientific Publishing: Singapore, 2004.
(21) Liu, D.; Plischke, M. Monte Carlo studies of tethered membranes with attractive interactions. *Phys. Rev. A* **1992**, *45*, 7139.
(22) Kantor, Y.; Kremer, K. Excluded-volume interactions in tethered membranes. *Phys. Rev. E* **1993**, *48*, 2490.
(23) Abraham, F.; Kardar, M. Folding and unbinding transitions in tethered membranes. *Science* **1991**, *252*, 419.
(24) Hwa, T.; Kokufuta, E.; Tanaka, T. Conformation of graphite oxide membranes in solution. *Phys. Rev. A* **1991**, *44*, R2235.
(25) Lipowsky, R. The conformation of membranes. *Nature* **1991**, *349*, 475.
(26) Wen, X.; Garland, C. W.; Hwa, T.; Kardar, M.; Kokufuta, E.; Li, Y.; Orkisz, M.; Tanaka, T. Crumpled and collapsed conformation in graphite oxide membranes. *Nature* **1992**, *355*, 426.
(27) Spector, M. S.; Naranjo, E.; Chiruvolu, S.; Zasadzinski, J. A. Conformations of a tethered membrane: Crumpling in graphitic oxide? *Phys. Rev. Lett.* **1994**, *73*, 2867.
(28) Titelman, G. I.; Gelman, V.; Bron, S.; Khalfin, R. L.; Cohen, Y.; Bianco-Peled, H. Characteristics and microstructure of aqueous colloidal dispersions of graphite oxide. *Carbon* **2005**, *43*, 641.
(29) Koltonow, A. R.; Luo, C.; Luo, J.; Huang, J. Graphene oxide sheets in solvents: To crumple or not to crumple? *ACS Omega* **2017**, *2*, 8005.
(30) Xu, Y.; Pospisil, M. J.; Green, M. J. The effect of bending stiffness on scaling laws for the size of colloidal nanosheets. *Nanotechnology* **2016**, *27*, 235702.
(31) Yllanes, D.; Bhabesh, S. S.; Nelson, D. R.; Bowick, M. J. Thermal crumpling of perforated two-dimensional sheets. *Nat. Commun.* **2017**, *8*, 1381.
(32) Espanol, P.; Warren, P. B. Perspective: Dissipative particle dynamics. *J. Chem. Phys.* **2017**, *146*, 150901.
(33) Hoogerbrugge, P.; Koelman, J. Simulating microscopic hydrodynamic phenomena with dissipative particle dynamics. *Europhys. Lett.* **1992**, *19*, 155.
(34) Symeonidis, V.; Karniadakis, G. E.; Caswell, B. Dissipative particle dynamics simulations of polymer chains: Scaling laws and shearing response compared to DNA experiments. *Phys. Rev. Lett.* **2005**, *95*, 076001.
(35) Pivkin, I. V.; Karniadakis, G. E. Accurate coarse-grained modeling of red blood cells. *Phys. Rev. Lett.* **2008**, *101*, 118105.
(36) Fedosov, D. A.; Pan, W.; Caswell, B.; Gompper, G.; Karniadakis, G. E. Predicting human blood viscosity in silico. *Proc. Natl. Acad. Sci. U. S. A.* **2011**, *108*, 11772.
(37) Xu, Z.; Peng, L.; Liu, Y.; Liu, Z.; Sun, H.; Gao, W.; Gao, C. Experimental guidance to graphene macroscopic wet-spun fibers, continuous papers, and ultralightweight aerogels. *Chem. Mater.* **2017**, *29*, 319.
(38) Groot, R.; Warren, P. Dissipative particle dynamics: Bridging the gap between atomistic and mesoscopic simulation. *J. Chem. Phys.* **1997**, *107*, 4423.
(39) Groot, R.; Rabone, K. Mesoscopic simulation of cell membrane damage, morphology change and rupture by nonionic surfactants. *Biophys. J.* **2001**, *81*, 725.
(40) Poulin, P.; Jalili, R.; Neri, W.; Nallet, F.; Divoux, T.; Colin, A.; Aboutalebi, S. H.; Wallace, G.; Zakri, C. Superflexibility of graphene oxide. *Proc. Natl. Acad. Sci. U. S. A.* **2016**, *113*, 11088.
(41) Plimpton, S. Fast parallel algorithms for short-range molecular dynamics. *J. Comput. Phys.* **1995**, *117*, 1.
(42) Boromand, A.; Jamali, S.; Maia, J. M. Viscosity measurement techniques in dissipative particle dynamics. *Comput. Phys. Commun.* **2015**, *196*, 149.
(43) Arkin, H.; Janke, W. Gyration tensor based analysis of the shapes of polymer chains in an attractive spherical cage. *J. Chem. Phys.* **2013**, *138*, 054904.

https://dx.doi.org/10.1021/acs.macromol.0c01425
Macromolecules 2020, 53, 10421−10430

(44) Shrake, A.; Rupley, J. A. Environment and exposure to solvent of protein atoms. Lysozyme and insulin. *J. Mol. Biol.* **1973**, *79*, 351.
(45) Fraaije, J.; van Male, J.; Becherer, P.; Serral Gracia, R. Calculation of diffusion coefficients through coarse-grained simulations using the automated-fragmentation-parametrization method and the recovery of Wilke-Chang statistical correlation. *J. Chem. Theory Comput.* **2018**, *14*, 479.
(46) Loman, A.; Gregor, I.; Stutz, C.; Mund, M.; Enderlein, J. Measuring rotational diffusion of macromolecules by fluorescence correlation spectroscopy. *Photochem. Photobiol. Sci.* **2010**, *9*, 627.
(47) Bowick, M. J.; Travesset, A. The statistical mechanics of membranes. *Phys. Rep.* **2001**, *344*, 255.
(48) Powers, T. R. Dynamics of filaments and membranes in a viscous fluid. *Rev. Mod. Phys.* **2010**, *82*, 1607.
(49) Babu, S. B.; Stark, H. Dynamics of semi-flexible tethered sheets : A simulation study using stochastic rotation dynamics. *Eur. Phys. J. E Soft Matter* **2011**, *34*, 136.
(50) Vovchenko, L.; Vovchenko, V. Simulation of percolation threshold in composites filled with conducting particles of various morphologies. *Materialwiss. Werkstofftech.* **2011**, *42*, 70.
(51) Mathew, M.; Schilling, T.; Oettel, M. Connectivity percolation in suspensions of hard platelets. *Phys. Rev. E* **2012**, *85*, 061407.
(52) Fasolino, A.; Los, J. H.; Katsnelson, M. I. Intrinsic ripples in graphene. *Nat. Mater.* **2007**, *6*, 858.
(53) Lindahl, N.; Midtvedt, D.; Svensson, J.; Nerushev, O. A.; Lindvall, N.; Isacsson, A.; Campbell, E. E. Determination of the bending rigidity of graphene via electrostatic actuation of buckled membranes. *Nano Lett.* **2012**, *12*, 3526.
(54) Wei, Y.; Wang, B.; Wu, J.; Yang, R.; Dunn, M. L. Bending rigidity and Gaussian bending stiffness of single-layered graphene. *Nano Lett.* **2013**, *13*, 26.
(55) Benedetti, I.; Nguyen, H.; Soler-Crespo, R. A.; Gao, W.; Mao, L.; Ghasemi, A.; Wen, J. G.; Nguyen, S.; Espinosa, H. D. Formulation and validation of a reduced order model of 2D materials exhibiting a two-phase microstructure as applied to graphene oxide. *J. Mech. Phys. Solids* **2018**, *112*, 66.
(56) Song, Z.; Xu, Z. Geometrical effect 'stiffens' graphene membrane at finite vacancy concentrations. *Extreme Mech. Lett.* **2016**, *6*, 82.
(57) den Otter, W. K.; Briels, W. J. The bending rigidity of an amphiphilic bilayer from equilibrium and nonequilibrium molecular dynamics. *J. Chem. Phys.* **2003**, *118*, 4712.
(58) Pan, J.; Tristram-Nagle, S.; Kucerka, N.; Nagle, J. F. Temperature dependence of structure, bending rigidity, and bilayer interactions of dioleoylphosphatidylcholine bilayers. *Biophys. J.* **2008**, *94*, 117.
(59) Danilov, D.; Barner-Kowollik, C.; Wenzel, W. Modelling of reversible single chain polymer self-assembly: From the polymer towards the protein limit. *Chem. Commun.* **2015**, *51*, 6002.
(60) Cranford, S. W.; Buehler, M. J. Packing efficiency and accessible surface area of crumpled graphene. *Phys. Rev. B* **2011**, *84*, 205451.
(61) Ortega, A.; García de la Torre, J. Hydrodynamic properties of rodlike and disklike particles in dilute solution. *J. Chem. Phys.* **2003**, *119*, 9914.
(62) Wang, Y.; Wang, S.; Li, P.; Rajendran, S.; Xu, Z.; Liu, S.; Guo, F.; He, Y.; Li, Z.; Xu, Z.; Gao, C. Conformational phase map of two-dimensional macromolecular graphene oxide in solution. *Matter* **2020**, *3*, 230.
(63) Tang, B.; Xiong, Z.; Yun, X.; Wang, X. Rolling up graphene oxide sheets through solvent-induced self-assembly in dispersions. *Nanoscale* **2018**, *10*, 4113.
(64) Tang, B.; Gao, E.; Xiong, Z.; Dang, B.; Xu, Z.; Wang, X. Transition of graphene oxide from nanomembrane to nanoscroll mediated by organic solvent in dispersion. *Chem. Mater.* **2018**, *30*, 5951.
(65) Koenig, S. P.; Boddeti, N. G.; Dunn, M. L.; Bunch, J. S. Ultrastrong adhesion of graphene membranes. *Nat. Nanotechnol.* **2011**, *6*, 543.
(66) Wen, Y.; Gao, E.; Hu, Z.; Xu, T.; Lu, H.; Xu, Z.; Li, C. Chemically modified graphene films with tunable negative Poisson's ratios. *Nat. Commun.* **2019**, *10*, 2446.
(67) Xin, G.; Zhu, W.; Deng, Y.; Cheng, J.; Zhang, L.; Chung, A.; De, S.; Lian, J. Microfluidics-enabled orientation and microstructure control of macroscopic graphene fibres. *Nat. Nanotechnol.* **2019**, *14*, 168.
(68) Homaeigohar, S.; Elbahri, M. Graphene membranes for water desalination. *NPG Asia Mater.* **2017**, *9*, No. e427.
(69) Ma, J.; Wang, P.; Dong, L.; Ruan, Y.; Lu, H. Highly conductive, mechanically strong graphene monolith assembled by three-dimensional printing of large graphene oxide. *J. Colloid Interface Sci.* **2019**, *534*, 12.
(70) Geng, H.; Yao, B.; Zhou, J.; Liu, K.; Bai, G.; Li, W.; Song, Y.; Shi, G.; Doi, M.; Wang, J. Size fractionation of graphene oxide nanosheets via controlled directional freezing. *J. Am. Chem. Soc.* **2017**, *139*, 12517.

https://dx.doi.org/10.1021/acs.macromol.0c01425
Macromolecules 2020, 53, 10421−10430